Contents lists available at ScienceDirect

Physics Letters B

Letter

New model based on coupling the Master and Langevin equations in the study of multinucleon transfer reactions

Long Zhu [a,b], [iD],*

[a] *Sino-French Institute of Nuclear Engineering and Technology, Sun Yat-sen University, Zhuhai 519082, China*
[b] *Guangxi Key Laboratory of Nuclear Physics and Nuclear Technology, Guangxi Normal University, Guilin 541004, China*

ARTICLE INFO

ABSTRACT

The multinucleon transfer process plays a crucial role for accessing unexplored isotopes far from the β-stable line. Developing reliable models is always one of biggest challenges for understanding the mechanism of the multinucleon transfer (MNT) process and providing accurate predictions. In this work, a new model, combining the Master and Langevin equations (CML), is developed for investigating the mechanism of the MNT reactions. The reaction ^{136}Xe+^{208}Pb is studied. The CML calculations are in rather good agreement with the experimental data. The effects of the incident energy and the entrance angular momentum on the production cross sections are investigated. One intriguing phenomenon is found that the dependence of the incident energy on the production yields in symmetry region is more intense than that for producing trans-target fragments.

Heavy-ion collisions around the Coulomb barrier are one of most rapidly developing field in nuclear physics and always attract a lot of attention due to the fact of offering numerous possibilities, such as synthesis of superheavy elements [1–6], production of isotopes far from the β stability line [7–12], as well as illuminating the equilibrium mechanism of quantum many-body system [13–15].

Because of the large variance of mass (charge), the multinucleon transfer (MNT) process is one promising approach to produce exotic nuclei [13] as well as the nuclei on the island of stability [16]. In particular, it was demonstrated that the MNT process shows great advantages of cross sections for producing neutron-rich isotopes which contributes significantly to the understanding of the r-process and shell evolution with large neutron excess [16–20]. However, the mechanism of the MNT process is still not clear, which also inhibits the production of unknown isotopes effectively.

One of the biggest challenges for understanding the mechanism of deep inelastic collisions and producing these unknown isotopes is lack of the theoretical model which could describe the possible reaction channels simultaneously. Developing new methods is essential and always desirable for better understanding the mechanism of the MNT and presenting more useful information for producing new isotopes. In resent years, several models have been developed and widely used in studying the MNT reactions, such as the time-dependent Hartree-Fock approach (TDHF) [21–24], the quantum molecular dynamics (QMD)

type models [25,26], the GRAZING model [27–29], the dinuclear system (DNS) type models [30–35], and coupled Langevin equations [36–38]. The present models still have their own shortcomings. For example, in the DNS model, the radial evolution is frozen. This is because in the DNS concept the dissipation and nucleon transfer processes take place at the bottom of the potential pocket. Consequently, the interaction time is input instead of self-consistent consideration of evolution from contact to separation. Nevertheless, the evolution of the radial degree of freedom plays an important role in the heavy ion collisions, especially for the fusion process which is the only approach to synthesize the superheavy elements. Also, the potential energy in the DNS model is considered in a diabatic way. However, in the case of collisions near Coulomb barrier, the system has enough time to change its shape and single particles levels in order to keep nuclear density constant.

Despite the above disadvantages, the Master equation (ME) employed in the DNS model is one of the most suitable tools for describing the evolution of systems produced in deep inelastic collisions. The ME is a general linear equation for the probability density, in which the transfer of nucleon is described as an equilibrium process [39]. Considering the fact that the Langevin equation (LE) has been successfully used in describing the time evolution of macroscopic variables, including the radial degree of freedom not only in fission process [40,41] but also the heavy ion collisions around the Coulomb barrier [42,43], I propose a new model based on the coupling of the Master equation and

---

Langevin equations (CML). Therefore, we have the following set of 3 coupled equations for 3 degrees of freedoms $\{Z_1, N_1, R\}$:

$$\frac{dP(Z_1, N_1)}{dt} =$$

$$\sum_{Z_1'} W_{Z_1, N_1; Z_1', N_1}(R) \left[d_{Z_1, N_1} P(Z_1', N_1) - d_{Z_1', N_1} P(Z_1, N_1) \right]$$

$$+ \sum_{N_1'} W_{Z_1, N_1; Z_1, N_1'}(R) \left[d_{Z_1, N_1} P(Z_1, N_1') - d_{Z_1, N_1'} P(Z_1, N_1) \right]; \quad (1)$$

$$\frac{dR}{dt} = \frac{p_R}{\mu_R};$$

$$\frac{dp_R}{dt} = -\frac{\partial V(R, J)}{\partial R} - \gamma_R \frac{p_R}{\mu_R} + \sqrt{\gamma_R T} \Gamma_R(t).$$

Here, $P(Z_1, N_1)$ is the distribution probability for the projectile-like fragment (PLF) with the proton number Z_1 and the neutron number N_1. At each moment, the evolution of radial degree (R) is described by the Langevin equations for the effective fragment combination of (A_1^m, Z_1^m; A_2^m, Z_2^m). Here, A_i^m and Z_i^m are respectively the average mass number and charge number of the ith nascent fragments based on the distribution probability $P(Z_i, N_i)$ calculated by using the Master equation. $A_i^m = \sum_{Z_i, N_i} (Z_i + N_i) \times P(Z_i, N_i)$, $Z_i^m = \sum_{Z_i, N_i} Z_i \times P(Z_i, N_i)$. $\mu_R = A_1^m A_2^m / (A_1^m + A_2^m)$. The value of μ_R varies during the evolution due to the transfer and exchange of nucleons. $W_{Z_1, N_1; Z_1', N_1}(R)$ denotes the mean transition probability from the channel (Z_1, N_1) to (Z_1', N_1) [44]. It is similar to N_1. d_{Z_1', N_1} is the microscopic dimension corresponding to the macroscopic state (Z_1, N_1). The parameters in the Master equation are exactly same with those employed in the DNS model [10]. The dissipation of the relative angular momentum can be expressed as $dJ/dt = -\gamma_J / \mu_R \times (J - J_{st})$. $J_{st} = \frac{I_{\text{rel}}}{I_{\text{tot}}} J_0$. $J_0 = L_0 \hbar$ is the initial entrance angular momentum set at the beginning of the collision. $\gamma_{R,J} = \gamma_{R,J}^0 F(\xi - \rho_F)$, $F(\zeta) = (1 + e^\zeta)^{-1}$, $\zeta = (\xi - \rho_F)/a_F$. $\xi = R - R_{\text{contact}}$. $a_F = 0.6$ fm; $\rho_F = 3$ fm; $\gamma_R^0 = 15 \times 10^{-21}$ MeV s fm^{-2}; $\gamma_J^0 = 30 \times 10^{-22}$ MeV s fm^{-2}. Above parameters related to the frictions $\gamma_{R,J}$ are determined by comparing the calculated mass distribution in the reaction ^{136}Xe + ^{208}Pb at $E_{\text{c.m.}} = 526$ MeV with the experimental data, as shown in Fig. 3 (a). $\Gamma_R(t)$ is a random force satisfying $<\Gamma_R(t)> = 0$ and $<\Gamma_R(t)\Gamma_R(t')> = 2\delta(t - t')$. $T = \sqrt{E_{\text{diss}}/a}$ standing for the temperature of the system. E_{diss} and a are the energy dissipated into the internal of the system and level density parameter respectively. In this work, the initial distance between projectile and the target is set as 30 fm. And the initial momentum can be determined based on the incident energy and the interaction potential. In the exit channel, the separation takes place and the simulation ends at $R = 50$ fm.

The cross section for kth collision event can be calculated naturally as follows:

$$\sigma_k(Z_1, N_1) = \frac{\pi \hbar^2}{2\mu E_{\text{c.m.}}} \sum_{L_0=0}^{L_{\text{max}}} (2L_0 + 1) \times P(Z_1, N_1). \quad (2)$$

Here, L_{max} corresponds to the grazing collision, which depends on the incident energy. After simulations of N_{tot} events, the cross section can be calculated as

$$\sigma(Z_1, N_1) = \frac{1}{N_{\text{tot}}} \sum_{k=1}^{N_{\text{tot}}} \sigma_k(Z_1, N_1). \quad (3)$$

The potential V is calculated as follows [38]:

$$V(A_1, Z_1; A_2, Z_2; \text{shape}, R, J) = V_{\text{adiab}}(A, Z; \text{shape}) \times B(R)$$

$$+ V_{\text{diab}}(A_1, Z_1; A_2, Z_2; R)[1 - B(R)] + \frac{(J\hbar)^2}{2\zeta_{\text{rel}}}. \quad (4)$$

Here, $B(R) = \left[1 + \exp\left(\frac{R - R_{\text{contact}}}{a_{\text{diff}}} \right) \right]^{-2}$, which defines transition from the properties of two separated nuclei to those of the mononucleus. $a_{\text{diff}} = 0.5$ fm [37]. The last term is centrifugal potential [10]. The adiabatic potential energy is defined as a difference between the mass of the whole nuclear system and the ground-state masses of the target and the projectile,

$$V_{\text{adiab}}(A, Z; \text{shape}) = M(A, Z; \text{shape})$$

$$- M(A_T, Z_T; \delta_T^{\text{g.s.}}) - M(A_P, Z_P; \delta_P^{\text{g.s.}}). \quad (5)$$

The finite-range liquid-drop model is used to calculate the macroscopic mass [45], which has the form

$$M(A, Z; \text{shape})|_{\eta_A = \eta_Z}$$

$$= m_p Z + m_n N - a_v (1 - k_v I^2) A$$

$$+ a_s (1 - k_s I^2) B_N(\vec{q}) A^{2/3} + \frac{3}{5} \frac{e^2 Z^2}{r_0 A^{1/3}} B_C(\vec{q})$$

$$- \frac{3}{4} \frac{e^2}{r_0} \left(\frac{9Z^4}{4\pi^2 A} \right)^{1/3} + f(k_F r_p) \frac{Z^2}{A} - c_a(N - Z) + a_0$$

$$+ W \left(|I| + \left\{ \begin{array}{ll} 1/A, & Z \text{ and } N \text{ equal and odd} \\ 0, & \text{otherwise} \end{array} \right\} \right)$$

$$+ \left\{ \begin{array}{ll} \bar{\Delta}_p + \bar{\Delta}_n - \delta_{np}, & Z \text{ and } N \text{ odd} \\ \bar{\Delta}_p, & Z \text{ odd and } N \text{ even} \\ \bar{\Delta}_n, & Z \text{ even and } N \text{ odd} \\ 0, & Z \text{ and } N \text{ even} \end{array} \right\}$$

$$- a_{\text{el}} Z^{2.39}. \quad (6)$$

$\eta_A (= (A_2 - A_1)/(A_2 + A_1))$ and $\eta_Z (= (Z_2 - Z_1)/(Z_2 + Z_1))$ are mass and charge asymmetries between target-like and projectile-like parts of the dissipation system. The terms in this formula are respectively the masses of Z protons and N neutrons; the volume energy; the surface energy and the Coulomb energy depending on deformation via the dimensionless functionals B_N and B_C, respectively; the Coulomb exchange correction; the proton form-factor correction to the Coulomb energy; the charge-asymmetry energy; the constant term; the Wigner energy; the average pairing energy; and the energy of bound electrons. The values of parameters in the finite-range liquid-drop model are exactly same with those in Ref. [45].

For an arbitrary value of η_Z, the macroscopic mass for the collision system can be calculated as follows:

$$M(A, Z; \text{shape}) = M(A, Z; \text{shape})|_{\eta_A = \eta_Z}$$

$$- C_{\eta_Z} \frac{(\eta_A - \langle \eta_Z \rangle)^2}{2} + C_{\eta_Z} \frac{(\eta_Z - \langle \eta_Z \rangle)^2}{2}. \quad (7)$$

Here, C_{η_Z} and $\langle \eta_Z \rangle$ can be written as [36,37],

$$C_{\eta_Z}(A, Z; \text{shape}) = \frac{2c_s Z_{CN}^2 (1+k)^2}{k A_{CN}} + \frac{(1+k)^2 E_C^0}{2k^2}$$

$$\times \left[(1+k)(B_C^1 + k B_C^2) - k B_C \right]$$

$$\langle \eta_Z \rangle (A, Z; \text{shape}) = \frac{(1+k)^2}{2k^2 A_{CN} C_{\eta_Z}} \left\{ 4c_s k Z_{CN}^2 \eta_A + E_C^0 A_{CN} \right.$$

$$\left. \times \left[B_C^1 - k^2 B_C^2 \right] \right\}, \quad (8)$$

where, $k = A_1/A_2$. A_{CN} and Z_{CN} are the mass and charge numbers of the collision system. E_C^0 is the Coulomb energy of the spherical compound nucleus. $c_s = 23.7$ MeV is the coefficient of the symmetry energy. B_C^i is the dimensionless functionals depending on deformation with respect to the spherical Coulomb energy for the ith nascent fragment.

The two center shell model is used to describe the shape of the system. We consider the axially symmetric ellipsoids, centered at z_i with semiaxes a_i and b_i ($i = 1, 2$) (see Fig. 1 (a)). R is the distance between two oscillator centers $R = z_2 - z_1$. The neck parameter in this work is $\epsilon = 0.35$. The projectile ^{136}Xe and target ^{208}Pb are spherical. The
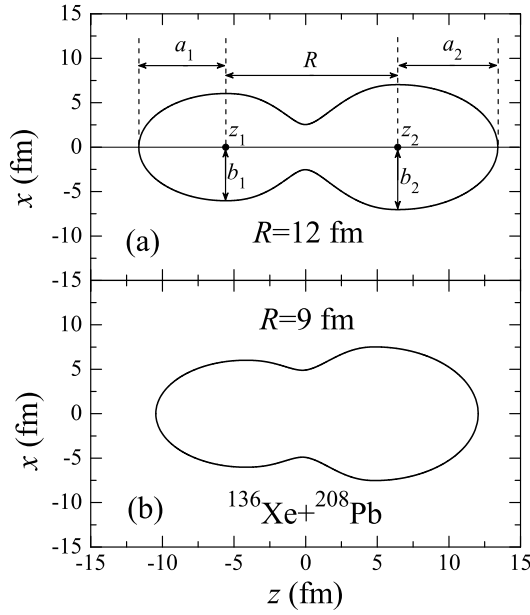
Fig. 1. Calculated shape contours of two interacting nuclei (^{136}Xe+^{208}Pb) in adiabatic way of collisions for $R = 12$ (a) and 9 fm (b). The parametrization of shape is denoted in panel (a).

Fig. 2. The calculated interaction potential as a function of the relative distance R for the reaction ^{136}Xe+^{208}Pb in diabatic (dashed line) and adiabatic (solid line) ways.

dynamical deformation of PLF and target like fragments during the evolution can be seen clearly. As shown in Fig. 1 (b), the growth of the neck takes place with decreasing value of R. In the case of near barrier collisions, the collision system has enough time to change their shape and keep the density constant.

The following definition is used for the diabatic potential energy V_{diab}:

$$V_{\text{diab}}(A_1, Z_1; A_2, Z_2; R) = V_{12}(A_1, Z_1; A_2, Z_2; R)$$
$$+ M\left(A_1, Z_1; \delta_1\right) + M\left(A_2, Z_2; \delta_2\right) \tag{9}$$
$$- M\left(A_T, Z_T; \delta_T^{\text{g.s.}}\right) - M\left(A_P, Z_P; \delta_P^{\text{g.s.}}\right).$$

The effective nucleus-nucleus interaction potential V can be written as

$$V_{12}(A_1, Z_1; A_2, Z_2; R) = V_N\left(A_1, Z_1; A_2, Z_2; R\right)$$
$$+ V_C\left(A_1, Z_1; A_2, Z_2; R\right). \tag{10}$$

Here, the Coulomb potential is taken as the form in Ref. [46],

$$V_C\left(A_1, Z_1; A_2, Z_2; R\right)$$
$$= \frac{Z_1 Z_2 e^2}{R} + \sqrt{\frac{9}{20\pi}}\left(\frac{Z_1 Z_2 e^2}{R^3}\right) \sum_{i=1,2} R_i^2 \beta_2^{(i)} P_2\left(\cos\theta_i\right) \tag{11}$$
$$+ \left(\frac{3}{7\pi}\right)\left(\frac{Z_1 Z_2 e^2}{R^3}\right) \sum_{i=1,2} R_i^2 \left[\beta_2^{(i)} P_2\left(\cos\theta_i\right)\right]^2.$$

The nuclear potential is taken the form as [47]

$$V_N\left(A_1, Z_1; A_2, Z_2; R\right)$$
$$= C_0 \left\{ \frac{F_{\text{in}} - F_{\text{ex}}}{\rho_0}\left[\int \rho_1^2(\mathbf{r})\rho_2(\mathbf{r} - \mathbf{R})d\mathbf{r}\right.\right.$$
$$+ \int \rho_1(\mathbf{r})\rho_2^2(\mathbf{r} - \mathbf{R})d\mathbf{r} \tag{12}$$
$$\left.\left. + F_{\text{ex}} \int \rho_1(\mathbf{r})\rho_2(\mathbf{r} - \mathbf{R})d\mathbf{r}\right]\right\}.$$

The detailed description of each term can be seen in Ref. [48]. The values of the parameters are exactly same with those in Ref. [37,47,48].

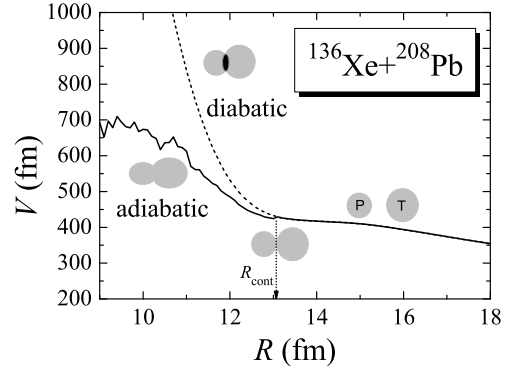Fig. 2 shows the interaction potential as a function of relative distance in the reaction ^{136}Xe+^{208}Pb. It can be seen that $V_{\text{diab}} = V_{\text{adiab}}$ for the two separated nuclei ($R > 13$ fm). However, after contact the interaction potential increases strongly for the diabatic case, which results from the doubling of the density. In this case, the strongly repulsive core in the potential could re-separate the collision partners in a very short time. The diabatic potential is only suitable for the collisions when the approaching speed of two nuclei is fast and comparable with nucleons speed in the nuclei. On the other hand, one can see that adiabatic potential calculated with the CML model obviously differs from the diabatic one after passing the contact point. The interaction potential increases gently because of rearrangement of the nucleons in the neck region.

Fig. 3 (a) shows the calculated mass distributions of the primary fragments with total kinetic energy loss (TKEL) greater than 40 MeV in the multinucleon transfer reaction ^{136}Xe + ^{208}Pb at incident energies $E_{\text{c.m.}} = 423, 526,$ and 617 MeV by using the CML model. The thick solid lines and thin dashed lines denote the results of the two-body events excluding the sequential fission of the heavy fragments and the results of all events, respectively. The statistical model as described in Ref. [35] is employed to perform the de-excitation process. The experimental data [49] are also shown, in which the events with the fission of the heavy fragments after the primary interaction are excluded. It can be seen the calculated results are in good agreement with the experimental data. The calculations show the same trend in cross sections with incident energy as observed in the experimental data, where the total cross sections increase as the incident energy rises. Another intriguing phenomenon is also found in both experimental data and the calculations (both cases) that the influence of the incident energy on the production yields in the symmetry region is more intense than that for producing asymmetry fragments, especially for high incident energies of 526 MeV and 617 MeV. This is because mass equilibrium effects which is related to the negative Q_{gg} values attract the system evolving symmetrically. However, for producing trans-target fragments, overcoming high potential energies results in the weak sensitivity to the incident energy. Therefore, for producing unknown isotopes in different regions, the optimal incident energies should be different. It is noticed that the DNS calculation couldn't reproduce this intriguing behavior [50]. The reproduction of the above experimental behaviors proves the reliability of the CML model. It is also worth to show the mass distribution for TKEL < 40 MeV. One can see the distribution is mainly around $A = 136$ and 208.

The results of all primary fragments (including the events with sequential fission) for different entrance angular momentums ($J = 20\hbar$, $200\hbar$, and $480\hbar$) at $E_{\text{c.m.}} = 526$ MeV are also shown in Fig. 3 (b). Clearly, as we expected that the fragments far from the projectile and target are mainly produced in collisions with small impact parameters, while the yields around the projectile and the target dominate in grazing collisions. The number of transferred nucleons strongly depends on the deepness of the contact as well as the interaction time. In order to
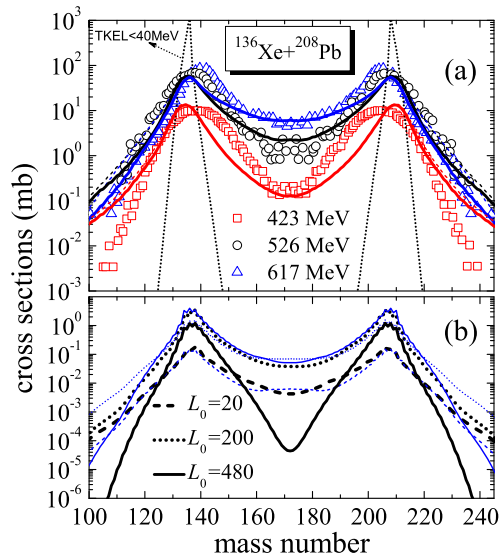
Fig. 3. (a) Mass distributions of primary products in the reaction ^{136}Xe+^{208}Pb with TKEL greater than 40 MeV at $E_{c.m.} = 423$, 526, and 617 MeV. The experimental data (denoted with symbols) are from Ref. [49]. The red, black, and blue lines denote the calculated results with the CML model for $E_{c.m.} = 423$, 526, and 617 MeV, respectively. The thick solid lines denote the results of the two-body events excluding the sequential fission of the heavy fragments. The thin dashed lines denote the results of all events. The dotted black line denotes the case of TKEL lower than 40 MeV at $E_{c.m.} = 526$ MeV. The coverage angular range of $40° < \theta_{c.m.} < 140°$ is taken into account. (b) The calculated production cross sections of all primary fragments for different incident angular momentum in the reaction ^{136}Xe+^{208}Pb with TKEL greater than 40 MeV. Thick black lines and thin blue lines denote the results at $E_{c.m.} = 526$ MeV and 617 MeV, respectively. The dashed, dotted, and solid lines denote the $J = 20\hbar$, $200\hbar$, and $480\hbar$ respectively.

clarify the incident energy effect on the mass distribution. I also show the results of $E_{c.m.} = 617$ MeV for comparison. It is found that the energy dependence is stronger for higher angular momentum. This is due to the fact that the wave function can be expanded to higher angular momentum for $E_{c.m.} = 617$ MeV. Consequently, comparing to incident energy of 526 MeV the cross section superiority of 617 MeV is obvious for $J = 480\hbar$. Hence, the behavior of the incident energy dependence as shown in Fig. 3 (a) is mainly contributed from the collisions in high entrance angular momentum.

The yields shown in Fig. 3 are mostly from the damped events. The values of TKEL are strongly related to the characteristics of the reaction channels. In order to further testify the CML model, I show the distributions of the TKEL for two-body events in the reaction ^{136}Xe + ^{208}Pb at $E_{c.m.} = 526$ MeV in Fig. 4. It can be seen that the CML results show very reasonable description of the TKEL distribution. The position of the TKEL equaling 40 MeV is shown. One can see that a significant portion of the yields are with TKEL lower than 40 MeV, which corresponds to the quasi-elastic collisions and the products around the projectile and target (see Fig. 3 (a)). The results from the DNS model are also shown. The DNS calculations underestimate the experimental data in the high TKEL region, which corresponds to the more damped collisions. Also, we can see that the quasi-elastic events corresponding to the low TKEL region are also strongly underestimated within the framework of the DNS model. Actually, the underestimation of the quasi-elastic events based on the ME in the DNS model has been recognized from the production cross sections of the fragments near the projectile-target [51]. In the CML model, the coupling of the LE strongly improves the description of the TKEL distribution.

In summary, one novel method, coupling the Master and Langevin equations (CML), is developed and presented in this work. The CML model achieves the purpose of mutual complementary advantages of
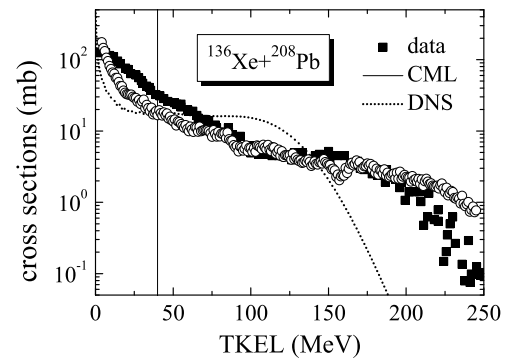
the LE and ME. Also, the CML model is applied in investigating the MNT reaction ^{136}Xe + ^{208}Pb. The incident energy and the entrance angular momentum effects on the cross sections are investigated. The calculations can reproduce the experimental data rather well. Furthermore, one intriguing phenomenon is found from both experimental data and the CML model calculations that the dependence of the incident energy on the production yields in the symmetry region is more intense than that for producing trans-target fragments. From view point of the partial waves, it is demonstrated that the behavior of the incident energy dependence on the production cross sections is mainly contributed from the collisions with high entrance angular momentum. This work could contribute significantly to the investigation of the MNT mechanism and production of unknown isotopes with exotic properties.

I would like to mention here, that Dr. P.W. Wen and his collaborators also have developed one novel model based on coupling the Master and Langevin equations [52].

Fig. 4. TKEL distributions of the primary fragments excluding the sequential fission of the heavy fragments in the reactions ^{136}Xe+^{208}Pb for $E_{c.m.} = 526$ MeV. The circles denote the calculated results from the CML model. The dotted line denotes the calculated result from the DNS model [50]. The vertical line denotes the position of TKEL equals 40 MeV. The experimental data are from Ref. [49].

Declaration of competing interest

The authors declare that they have no known competing financial interests or personal relationships that could have appeared to influence the work reported in this paper.

Data availability

No data was used for the research described in the article.

References

[1] S.A. Giuliani, Z. Matheson, W. Nazarewicz, E. Olsen, P.G. Reinhard, J. Sadhukhan, B. Schuetrumpf, N. Schunck, P. Schwerdtfeger, Rev. Mod. Phys. 91 (2019) 011001.
[2] S. Hofmann, G. Münzenberg, Rev. Mod. Phys. 72 (2000) 733.
[3] G. Münzenberg, M. Gupta, H.M. Devaraja, Y.K. Gambhir, S. Heinz, S. Hofmann, Eur. Phys. J. A 59 (2023) 21.
[4] Yu.Ts. Oganessian, V.K. Utyonkov, Nucl. Phys. A 944 (2015) 62–98.
[5] Yu.Ts. Oganessian, V.K. Utyonkov, Rep. Prog. Phys. 78 (2015) 036301.
[6] K. Morita, K. Morimoto, D. Kaji, H. Haba, K. Ozeki, Y. Kudou, T. Sumita, Y. Wakabayashi, A. Yoneda, K. Tanaka, S. Yamaki, R. Sakai, T. Akiyama, S. Goto, H. Hasebe, M. Huang, T. Huang, E. Ideguchi, Y. Kasamatsu, K. Katori, Y. Kariya, H. Kikunaga, H. Koura, H. Kudo, A. Mashiko, K. Mayama, S. Mitsuoka, T. Moriya, M.

Murakami, H. Murayama, S. Namai, A. Ozawa, N. Sato, K. Sueki, M. Takeyama, F. Tokanai, T. Yamaguchi, A. Yoshida, J. Phys. Soc. Jpn. 81 (2012) 103201.

[7] G. Adamian, N. Antonenko, A. Diaz-Torres, S. Heinz, Eur. Phys. J. A 56 (2020) 47.
[8] F.-S. Zhang, C. Li, L. Zhu, P.-W. Wen, Front. Phys. 13 (2018) 132113.
[9] W.D. Loveland, Front. Phys. 7 (2019) 23.
[10] L. Zhu, C. Li, C.-C. Guo, J. Su, P.-W. Wen, G. Zhang, F.-S. Zhang, Int. J. Mod. Phys. E 29 (2020) 2030004.
[11] H.M. Devaraja, S. Heinz, D. Ackermann, T. Göbel, F.P. Heßberger, S. Hofmann, J. Maurer, G. Münzenberg, A.G. Popeko, A.V. Yeremin, Eur. Phys. J. A 56 (2020) 224.
[12] K. Sekizawa, Front. Phys. 7 (2019) 20.
[13] V.V. Volkov, Phys. Rep. 44 (1978) 93.
[14] C. Simenel, K. Godbey, A.S. Umar, Phys. Rev. Lett. 124 (2020) 212504.
[15] Z. Liao, L. Zhu, J. Su, C. Li, Phys. Rev. C 107 (2023) 014614.
[16] L. Zhu, J. Su, C. Li, F.S. Zhang, Phys. Lett. B 829 (2022) 137113.
[17] V. Zagrebaev, W. Greiner, Phys. Rev. Lett. 101 (2008) 122701.
[18] L. Zhu, J. Su, W.J. Xie, F.S. Zhang, Phys. Lett. B 767 (2017) 437–442.
[19] Y.X. Watanabe, Y.H. Kim, S.C. Jeong, et al., Phys. Rev. Lett. 115 (2015) 172503.
[20] T. Niwase, Y.X. Watanabe, Y. Hirayama, M. Mukai, P. Schury, A.N. Andreyev, T. Hashimoto, S. Iimura, H. Ishiyama, et al., Phys. Rev. Lett. 130 (2023) 132502.
[21] K. Sekizawa, S. Ayik, Phys. Rev. C 102 (2020) 014620.
[22] Z. Wu, L. Guo, Z. Liu, G. Peng, Phys. Lett. B 825 (2022) 136886.
[23] S. Ayik, M. Arik, E.C. Karanfil, O. Yilmaz, B. Yilmaz, A.S. Umar, Phys. Rev. C 104 (2021) 054614.
[24] X. Jiang, N. Wang, Chin. Phys. C 42 (2018) 104105.
[25] K. Zhao, Z. Liu, F. Zhang, N. Wang, Phys. Lett. B 815 (2021) 136101.
[26] C. Li, P. Wen, J. Li, G. Zhang, B. Li, X. Xu, Z. Liu, S. Zhu, F.S. Zhang, Phys. Lett. B 776 (2018) 278.
[27] A. Winther, Nucl. Phys. A 572 (1994) 191.
[28] R. Yanez, W. Loveland, Phys. Rev. C 91 (2015) 044608.
[29] P.W. Wen, C.J. Lin, C. Li, L. Zhu, F. Zhang, F.S. Zhang, et al., Phys. Rev. C 99 (2019) 034606.
[30] L. Zhu, Z.Q. Feng, F.S. Zhang, J. Phys. G, Nucl. Part. Phys. 42 (2015) 085102.
[31] X.J. Bao, S.Q. Guo, J.Q. Li, H.F. Zhang, Phys. Lett. B 785 (2018) 221.
[32] Yu.E. Penionzhkevich, G.G. Adamian, N.V. Antonenko, Phys. Lett. B 621 (2005) 119–125.
[33] G.G. Adamian, N.V. Antonenko, V.V. Sargsyan, W. Scheid, Phys. Rev. C 81 (2010) 024604.
[34] P.W. Wen, A.K. Nasirov, C.J. Lin, H.M. Jia, J. Phys. G 47 (2020) 075106.
[35] L. Zhu, J. Su, Phys. Rev. C 104 (2021) 044606.
[36] A.V. Karpov, G.D. Adeev, Phys. At. Nucl. 65 (2002) 1596, Eur. Phys. J. A 14 (2002) 169.
[37] A.V. Karpov, V.V. Saiko, Phys. Rev. C 96 (2017) 024618.
[38] V. Zagrebaev, A. Karpov, Y. Aritomo, W. Naumenko, W. Greiner, Phys. Part. Nucl. 38 (2007) 469.
[39] W. Nörenberg, Phys. Lett. B 53 (1974) 289.
[40] L.L. Liu, X.Z. Wu, Y.J. Chen, C.W. Shen, Z.G. Ge, Z.X. Li, Phys. Rev. C 105 (2022) 034614.
[41] Y. Huang, Y. Feng, E. Xiao, X. Lei, L. Zhu, J. Su, Phys. Rev. C 106 (2022) 054606.
[42] V.I. Zagrebaev, W. Greiner, Nucl. Phys. A 944 (2015) 257–307.
[43] Z.H. Liu, J.D. Bao, Phys. Rev. C 89 (2014) 024604.
[44] W. Nörenberg, Z. Phys. A 274 (1975) 241.
[45] P. Möller, J.R. Nix, W.D. Myers, W.J. Swiatecki, At. Data Nucl. Data Tables 59 (1995) 185.
[46] C.Y. Wong, Phys. Rev. Lett. 31 (1973) 766.
[47] G.G. Adamian, N.V. Antonenko, R.V. Jolos, S.P. Ivanova, O.I. Melnikova, Int. J. Mod. Phys. E 5 (1996) 191–216.
[48] L. Zhu, Phys. Rev. Res. 5 (2023) L022030.
[49] E.M. Kozulin, E. Vardaci, G.N. Knyazheva, A.A. Bogachev, S.N. Dmitriev, I.M. Itkis, M.G. Itkis, A.G. Knyazev, T.A. Loktev, K.V. Novikov, et al., Phys. Rev. C 86 (2012) 044611.
[50] L. Zhu, P.W. Wen, C.J. Lin, X.J. Bao, J. Su, C. Li, C.C. Guo, Phys. Rev. C 97 (2018) 044614.
[51] L. Zhu, J. Phys. G, Nucl. Part. Phys. 46 (2019) 065102.
[52] P.W. Wen, private communication.